Diagnosing the Observed Seasonal Cycle of Atlantic Subtropical Mode Water Using Potential Vorticity and Its Attendant Theorems

GUILLAUME MAZE* AND JOHN MARSHALL

Department of Earth, Atmospheric, and Planetary Sciences, Massachusetts Institute of Technology, Cambridge, Massachusetts

ABSTRACT

Analyzed fields of ocean circulation and the flux form of the potential vorticity equation are used to map the creation and subsequent circulation of low potential vorticity waters known as subtropical mode water (STMW) in the North Atlantic. Novel mapping techniques are applied to (i) render the seasonal cycle and annual-mean mixed layer vertical flux of potential vorticity (PV) through outcrops and (ii) visualize the extraction of PV from the mode water layer in winter, over and to the south of the Gulf Stream. Both buoyancy loss and wind forcing contribute to the extraction of PV, but the authors find that the former greatly exceeds the latter. The subsequent path of STMW is also mapped using Bernoulli contours on isopycnal surfaces.

1. Introduction

The vertical structure of the subtropical gyre of the North Atlantic is marked by an anomalously thick layer of water with a mean temperature of 18°C, sandwiched between the permanent and seasonal thermocline. Known as Eighteen Degree Water (EDW),[1] its mean thickness is mapped out in Fig. 1.

Much progress has been made in quantifying and identifying key mechanisms of EDW formation and dissipation by viewing it through the water-mass transformation formalism of Walin (1982) (see, e.g., Speer and Tziperman 1992; Marshall et al. 1999; Maze et al. 2009; Forget et al. 2011, hereafter FG11). The Walin water-mass transformation framework focuses on integral statements, but it inspired Maze et al. (2009) to develop a mapping technique that allows one to visualize spatial patterns of formation induced by air–sea fluxes

(see also Brambilla et al. 2008). For example, in Fig. 1 we map the formation rate of EDW waters in the density range $\sigma = 26.4 \pm 0.2$ kg m^{-3} using the Ocean Comprehensive Atlas (OCCA) dataset (described in section 2a) during 2004–06. Positive regions indicate a convergence of volume flux between $\sigma = 26.4 \pm 0.2$ kg m^{-3} and hence an increase in the volume of EDW. As discussed in Maze et al., the EDW formation region is located between the Gulf Stream path and the core of EDW and can be seen in Fig. 1 (see the 2004–06 mean thickness of the EDW layer contoured in green). As concluded by Maze et al. (2009) and FG11, EDW formation is primarily driven by air–sea heat fluxes, which deepen the mixed layer just south of the Gulf Stream in wintertime, much as originally deduced by Worthington and collaborators (see Worthington 1959, 1972, 1976).

An important limitation of the Walin approach, however, is that it focuses on water within a particular density class, but without an additional constraint on properties such as, for example, potential vorticity (PV). One particularly important subset of EDW is subtropical mode water (STMW). STMW is EDW that also has weak stratification and hence low PV. Low PV is indicative of water whose characteristics have been recently reset by wintertime convection. Following Hanawa and Talley (2001) and subsequent studies from Kwon and Riser (2004) and FG11, here we define North Atlantic STMW as EDW with a potential vorticity of $Q < 1.5 \times 10^{-10}$ m^{-1} s^{-1}. How then do we write down budgets for this particular water mass? What are the respective

---

[1] Here we define EDW as all water in a density range $\sigma = 26.4 \pm 0.2$ kg m^{-3} (roughly corresponding to temperature between 17° and 19°C) and STMW as EDW with a potential vorticity less than 1.5×10^{-10} m^{-1} s^{-1}. For a detailed discussion see FG11.

---

* Current affiliation: Laboratoire de Physique des Océans, IFREMER, Plouzané, France.

Corresponding author address: Guillaume Maze, Laboratoire de Physique des Océans, IFREMER, BP70, 29280 Plouzané, France.
E-mail: gmaze@ifremer.fr
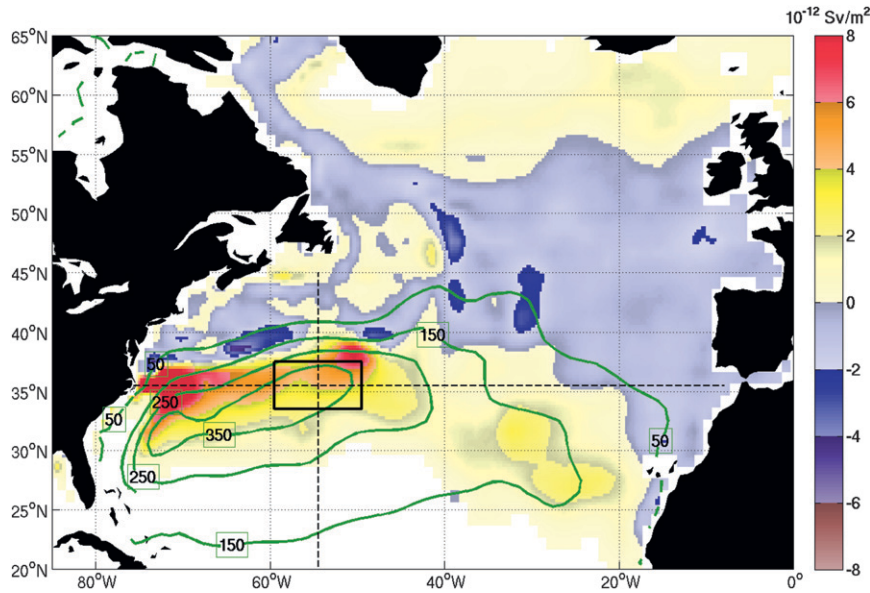
FIG. 1. The 2004–06 mean EDW formation rate (color shading) map due to surface buoyancy fluxes [unit is 10^{-12} Sv m^{-2} = 10^{-6} m s^{-1} (Sv $\equiv 10^6$ m^3 s^{-1})]. A positive formation rate corresponds to an increase in the volume of EDW. Here EDW is defined to be the density class σ = 26.4 ± 0.2 kg m^{-3}. Green contours are the 2004–06 mean EDW layer thickness in meters. Zonal and meridional black dashed lines mark the locations of PV sections shown in Figs. 3 and 4. The solid black box at their intersection marks the region over which spatial averages are taken in Fig. 6.

contributions of diabatic and mechanical (wind) forcing to its formation process?

In this paper, we use potential vorticity and its attendant theorems to analyze and quantify the creation and circulation of North Atlantic STMW. We make use of the OCCA dataset obtained by employing an ocean model to interpolate near-global Argo, SST, and altimetric datasets collected over a 3-yr period from 2004 to 2006 (Forget 2010). In section 2, we describe the observed mixed layer evolution and PV signature of STMW over the seasonal cycle. In section 3, we present the theoretical background of our study, reviewing the "flux form" of the PV equation, PV flux (**J**) vectors and the "impermeability theorem." In section 4, we map the interior PV flux in the EDW layer, making use of the impermeability theorem and the vertical PV flux through the sea surface. We also discuss the relative contribution of buoyancy and mechanical wind forcing in PV extraction. In section 5, we discuss and conclude.

2. The seasonal cycle of subtropical model water in the North Atlantic

a. Ocean state estimate employed

To map entry, flux, and exit of potential vorticity in mode water formation we use the Ocean Comprehensive

Atlas, a global state estimate of the ocean providing daily fields at a horizontal resolution of 1° × 1° with 50 vertical levels (Forget 2010). It was produced using the Massachusetts Institute of Technology general circulation model (MITgcm) (Marshall et al. 1997a,b) data assimilation technology, which fits the model trajectory to contemporary global datasets, particularly Argo profiles of temperature and salinity, surface altimetry, and satellite SSTs (ECCO) (Wunsch and Heimbach 2007). The model is fit to the data year by year using adjoint techniques with overlapping windows to deal with the join. This procedure yields a dynamically consistent global ocean state estimate, which is notable for its closeness to the observations and its limited temporal drift. OCCA was used to study the seasonal cycle of Eighteen Degree Water in the North Atlantic in Maze et al. (2009) and FG11. The reader is referred to the aforementioned papers for further details about OCCA, its strengths and limitations.

b. Evolution of the mixed layer depth over the seasonal cycle

STMW is characterized by weak stratification and hence low potential vorticity. We thus begin our discussion by describing the seasonal cycle of vertical mixing and restratification by presenting monthly-mean fields
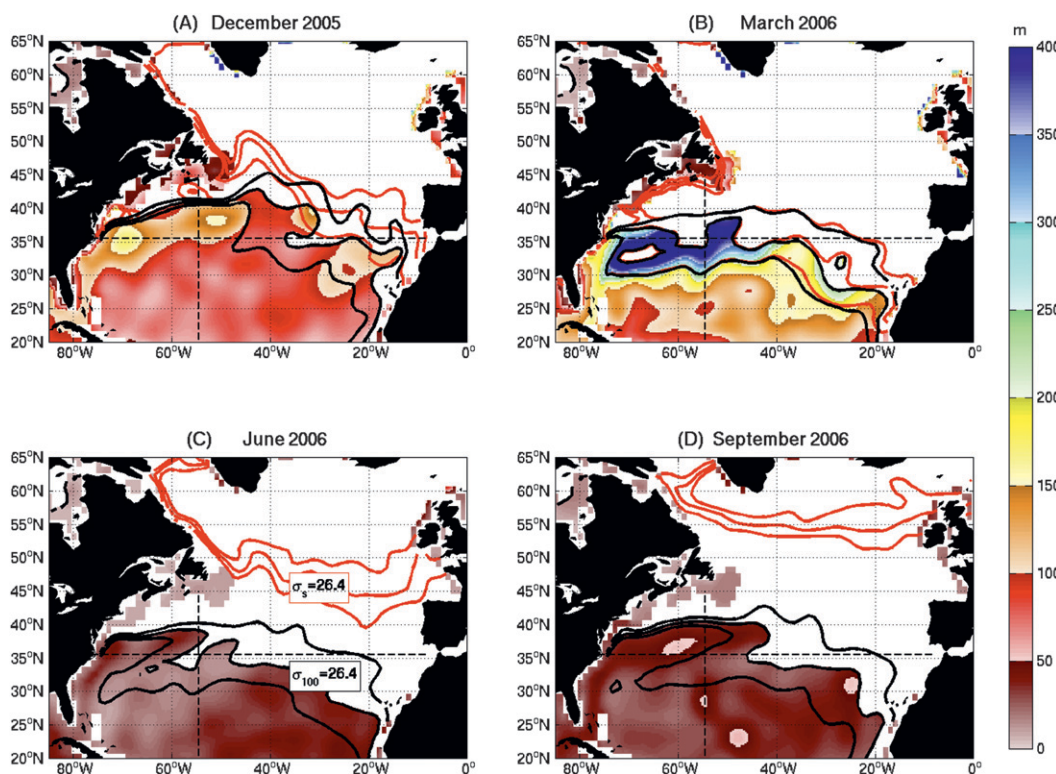
FIG. 2. Monthly mean mixed layer depth for December 2005 and March, June, and September 2006 with $\sigma = 26.4 \pm 0.2$ kg m^{-3} outcrops at the surface (red) and at a depth of 100 m (black) superimposed. Fields are blanked out if $\sigma > 26.4$ kg m^{-3} at a depth of 100 m.

four times during a typical year (2006): December 2005 and March, June, and September 2006. Figure 2 shows the mixed layer depth (MLD): note that areas where $\sigma > 26.4$ kg m^{-3} at a depth of 100 m have been blanked out. This highlights the region of STMW ventilation. In December 2005 the ML is between a depth of 50 and 100 m over most of the subtropical gyre, except south of the Gulf Stream. Here, wintertime storms have begun to advect very cold air masses from the continent over the warmer ocean south of the Gulf Stream (see, e.g., the review in Marshall et al. 2009). Strong winds and large air–sea temperature differences induce very high buoyancy losses, triggering overturning and driving the mixed layer to depths from 100 to 175 m. In March 2006, air–sea temperature differences and wind stress amplitudes reach a maximum and the MLD exceeds 100 m over the whole basin. At this time outcrops of the $\sigma = 26.4 \pm 0.2$ kg m^{-3} at the surface and at a depth of 100 m lie almost on top of one another (see the black and red contours).[2] This indicates that the mixed layer has

penetrated the core of STMW, thus replenishing its low stratification and potential vorticity (see section 2c). South of the Gulf Stream, we observe the deepest mixed layers over the seasonal cycle, reaching 400 m or so. In June and September 2006 the restratification induced by buoyancy gain at the sea surface and advective processes lead to the formation of the seasonal thermocline and the ML shoals to less than 50 m. Note that, although the $\sigma = 26.4 \pm 0.2$ kg m^{-3} surface outcrops have migrated northward (red contours), outcrops at a depth of 100 m have not moved significantly from their March 2006 position.

c. Observed PV signature of mode water

STMW is a subset of the larger EDW layer that has low PV defined by a PV amplitude threshold. The closer to zero this threshold value is, the most recently ventilated is the subset of water mass is thus defined and the smaller its volume. Many studies use different threshold values, and this has led to confusion when comparing estimates of mode water volumes and formation rates, as discussed at length by FG11. Here we choose to label STMW with a PV value of 1.5×10^{-10} m^{-1} s^{-1} because it serves to isolate the most recently ventilated waters

---

[2] In this study, the term "outcrop" refers to the two-dimensional horizontal area between two isopycnal contours at any given depth, not only the sea surface.
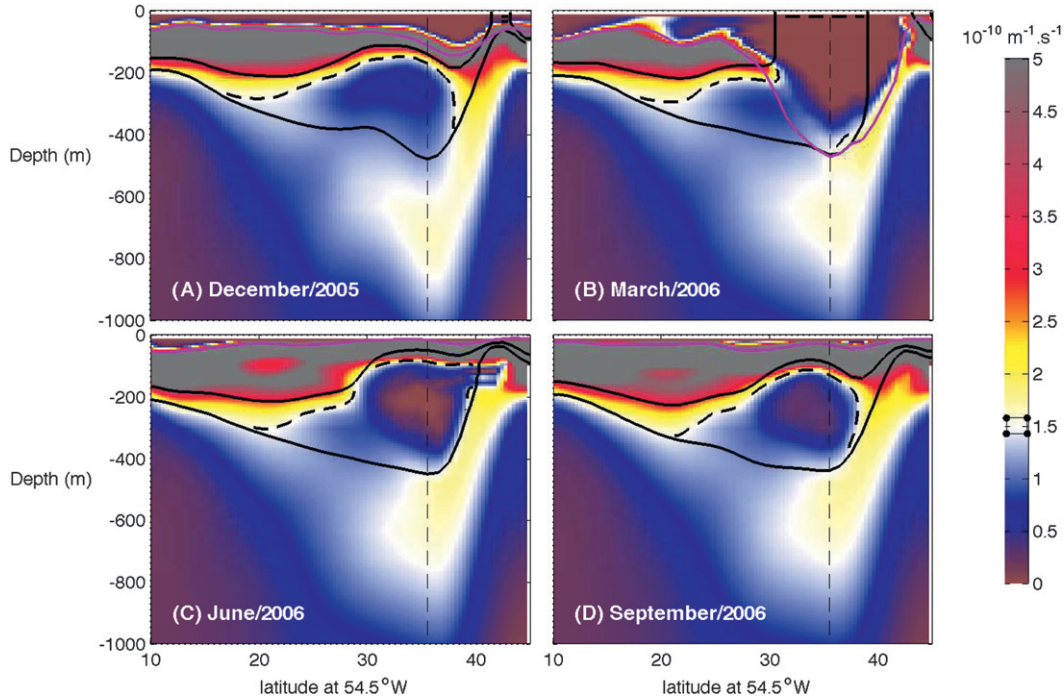
FIG. 3. Meridional section along 54.5°W (indicated in Figs. 1, 2) of the monthly-mean potential vorticity Q given by Eq. (1) (color shading), isopycnals defining EDW $\sigma_\theta = 26.4 \pm 0.2$ kg m^{-3} (black) and MLD (magenta). The STMW subset of EDW with $Q \leq 1.5 \times 10^{-10}$ m^{-1} s^{-1} is marked by the black dashed contour within the EDW layer (corresponding to white color shading). The position of the zonal section from Fig. 4 is shown as a thin black dashed vertical line. Monthly-mean fields are shown for (a) December 2005, (b) March 2006, (c) June 2006, and (d) September 2006.

[note that it is the same value used by FG11 but is slightly less restrictive than the historical value of $Q < 10^{-10}$ m^{-1} s^{-1} used by McDowell et al. (1982) and Keffer (1985)].

The potential vorticity, thus defined as

$$Q \equiv -\frac{f}{\rho}\frac{\partial\sigma}{\partial z} \qquad (1)$$

(where the relative vorticity has been neglected, f is the Coriolis parameter, ρ the in situ density, and σ the potential density)[3], is plotted in Figs. 3 and 4 . Meridional and zonal sections for the same four months used in Fig. 2 are presented. Note that the EDW layer exists somewhere within the column at all horizontal positions in these sections (between the black density contours). STMW is much more restricted in extent (within the black dashed Q contours inside the EDW layer) owing to the PV criterion.

In December (Figs. 3a and 4a), STMW begins the winter season with a core PV value of roughly

0.7×10^{-10} m^{-1} s^{-1}. The mixed layer (magenta line) begins to erode the seasonal thermocline but has not yet broken through to the STMW layer. In March (Figs. 3b and 4b) the mixed layer now ventilates STMW along its northern flank. The STMW potential vorticity is several orders of magnitude smaller than its prewinter value. This is the time when the STMW core has its PV reset to very low values. In June (Figs. 3c and 4c) the EDW layer has become isolated from the sea surface by the seasonal thermocline and the subset of STMW has a significantly lower value of PV than in prewinter. By September (Figs. 3d and 4d) the situation is rather similar to the one in June except that the EDW/STMW layers have been "pushed" downward by the seasonal thermocline and the STMW potential vorticity has begun to increase in value.

Figure 5 shows maps of potential vorticity on the EDW isopycnal core $\sigma = 26.4$ kg m^{-3} for the same four months. In December (Fig. 5a), a very low PV core of STMW is clearly evident around 33°N, 55°W. Away from this core, the STMW (identified by the white contour) potential vorticity rapidly increases northward as the Gulf Stream front is approached. The STMW PV remains small, moving westward toward the coast. Eastward and

---

[3] Defined as $\sigma = \rho|_{p_{atm}} - 1000$ kg m^{-3} and usually referred to as σ_θ in the literature.
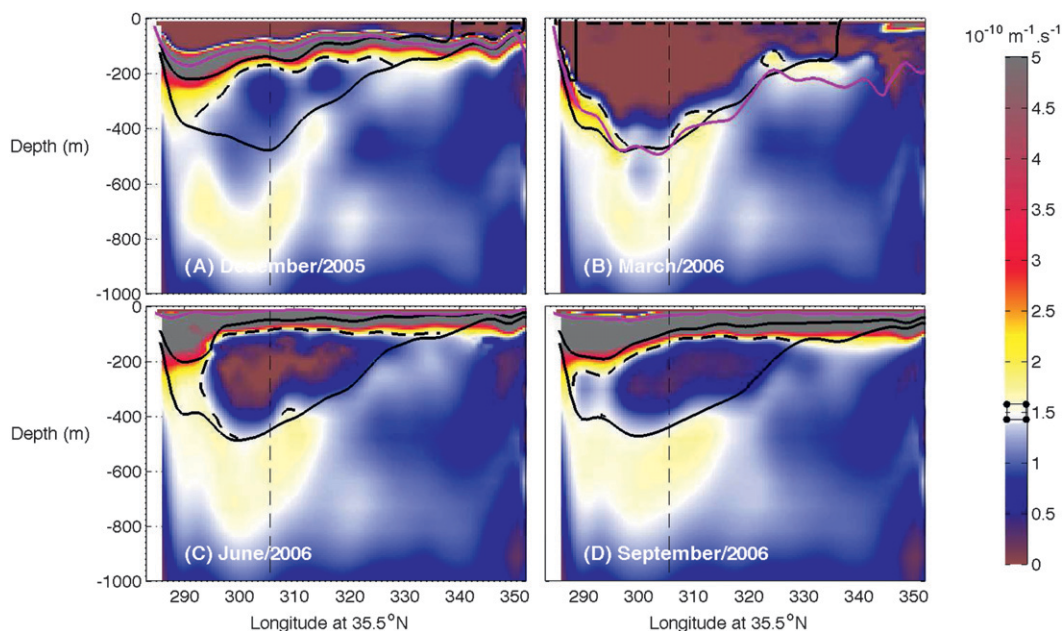
FIG. 4. As in Fig. 3 but for the zonal section at latitude 35.5°N. The position of the meridional section from Fig. 3 is indicated by the thin black dashed vertical line.

southward, the STMW PV increases as the thickness of the STMW layer decreases. In March (Fig. 5b), $\sigma = 26.4 \pm 0.2$ kg m^{-3} outcrops at the sea surface (red contours) and 100 m (black contours) are now coincident with one another. This indicates that the deepening mixed layer has broken through to the volume of STMW below (see Figs. 3b and 4b). The horizontal extent of this pattern also indicates that the mixed layer has accessed much of the STMW on its northern flank. Indeed, while the $\sigma = 26.6$ kg m^{-3} outcrop remains confined to the Gulf Stream path (roughly 38°N), the $\sigma = 26.2$ kg m^{-3} outcrop reaches 30°N between 75° and 40°W or so. In June (Fig. 5c), as buoyancy is gained, the EDW outcrop migrates northward while the outcrops at 100 m remain close to their March positions. This reveals the pronounced migration of EDW isopycnals that are confined to the seasonal thermocline, a migration primarily associated with air–sea buoyancy fluxes. The overall PV of STMW is now much smaller than its prewinter values. In September (Fig. 5d) EDW outcrops at 100 m have migrated slightly northward and the STMW PV magnitudes, although already slightly larger than in June, remain smaller than their prewinter levels.

3. Theoretical background: The flux form of the PV equation

In section 2 we mapped the observed distribution of STMW using potential vorticity. How, when, and where

was the PV of STMW formed, and what is its subsequent fate? We now briefly review the flux form of the PV equation and describe how it can be used to map the flux of PV to and from the EDW layer over the seasonal cycle and its circulation in the interior ocean.

The most familiar form of potential vorticity, Q, conservation is a Lagrangian statement of the form $DQ/Dt = $ sources $-$ sinks, where D/Dt is the Lagrangian derivative. Thus, in the absence of sources and sinks, the Q of a fluid parcel is conserved following that parcel around. Here, however, we made use of an alternative form of the PV equation, which is written in flux form. This is of particular utility in the present application because, rather than focus on the properties of a particular fluid parcel, it enables one to make statements about the budget of PV within a layer of fluid sandwiched between potential density, σ, surfaces. Moreover, we can make much use of constraints on the direction of PV flux: as remarkable as it may seem, there can be no flux of PV (in the generalized sense to be defined below) through σ surfaces. Thus, the only way of changing the PV within the layer is by frictional and/or buoyancy fluxes acting where the layer abuts surfaces—the sea surface and/or bathymetry/coast. We see then that the flux form of the PV equation is naturally—indeed perfectly—suited to budget for STMW (water of a particular PV) within an EDW layer sandwiched between two chosen σ surfaces. We now go on to review the relevant theory.
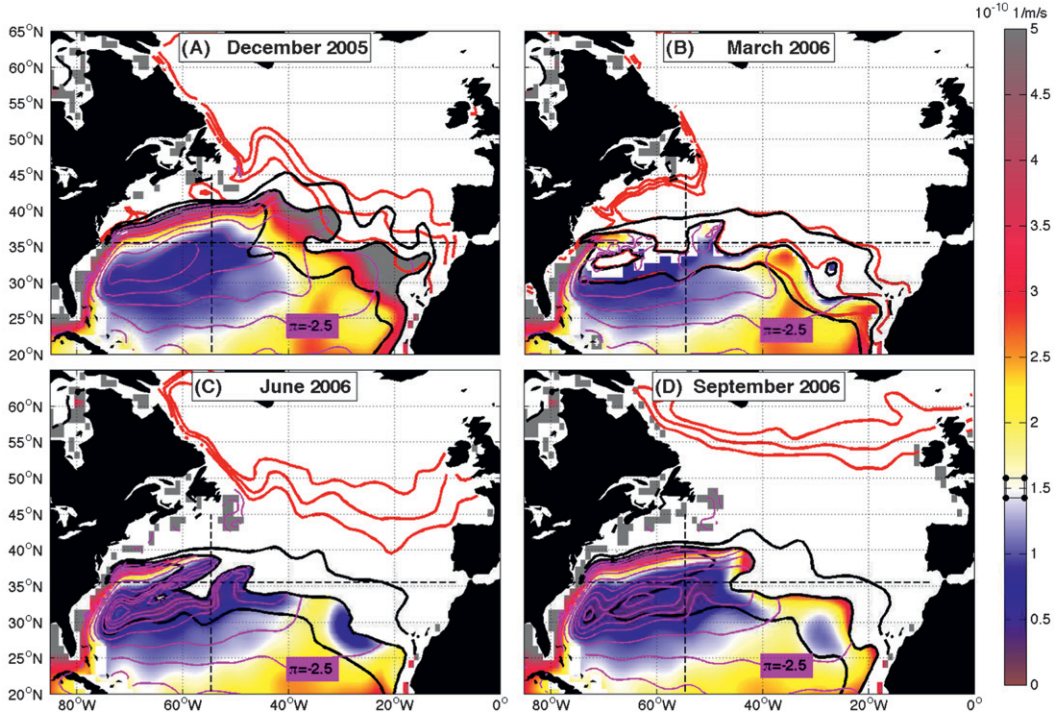
FIG. 5. Potential vorticity (color shading) on the $\sigma = 26.4$ kg m^{-3} STMW core isopycnal at depths below 100 m. The STMW PV threshold level $Q = 1.5 \times 10^{-10}$ m^{-1} s^{-1} corresponds to white. Thick red and black contours are $\sigma = 26.4 \pm 0.2$ kg m^{-3} outcrops at the surface and at 100-m depth. Magenta contours are isolines on the $\sigma = 26.4$ kg m^{-3} isopycnal of the Bernoulli function π, the streamfunction for the **J** vector. Contours are every 0.5 m^2 s^{-2}, increasing toward the center of the gyre. The $\pi = -2.5$ m^2 s^{-2} contour is labeled in the southeast part of the basin. Monthly mean fields are plotted for (a) December 2005 and (b) March, (c) June, and (d) September 2006.

Adopting the notation of Marshall et al. (2001, hereafter M01), the flux form of the potential vorticity equation can be written as

$$\frac{\partial}{\partial t}(\rho Q) + \nabla \cdot \mathbf{J} = 0, \tag{2}$$

where **J** is the aforementioned generalized flux of potential vorticity Q, representing the total advective and nonadvective transport of potential vorticity in the ocean. Its utility is that it puts advective and nonadvective (e.g., diffusive) fluxes on an equal footing. Here Q is the Ertel potential vorticity, defined by

$$Q = -\frac{1}{\rho}\omega \cdot \nabla \sigma \tag{3}$$

in which ρ is the in situ density, σ is the potential density, and

$$\omega = 2\Omega + \nabla \times \mathbf{u} \tag{4}$$

is the absolute vorticity with Ω the earth's rotation vector and **u** the fluid velocity.

As discussed at length in Marshall and Nurser (1992, hereafter MN92) and M01, the conservation law Eq. (2) has a number of notable properties:

(i) Because the mass-weighted PV can always be written as the divergence of a vector [from Eq. (3), $\rho Q = -\nabla \cdot (\omega \sigma)$], a flux-form PV equation, of the form Eq. (2), can always be written for an appropriate **J**, defined below.

(ii) The rhs of Eq. (2) is identically zero, even in the presence of sources of momentum and buoyancy. So, irrespective of whether Q is materially conserved, Eq. (2) always holds.

(iii) There is a constraint on the **J** vectors: **J** cannot pass through a σ surface. Thus, σ surfaces are impermeable to potential vorticity (Haynes and McIntyre 1987). This is known as the impermeability theorem.

The **J** vector can be written down in alternative and equivalent forms [see Eqs. (10) and (11) of M01—written here again for convenience:

$$\mathbf{J} = \omega \frac{\partial \sigma}{\partial t} + \left(\frac{\partial \mathbf{u}}{\partial t} + \nabla \pi\right) \times \nabla \sigma \tag{5}$$

or

$$\mathbf{J} = \rho Q \mathbf{u} + \omega \frac{D\sigma}{Dt} + \mathbf{F} \times \nabla \sigma + \frac{\Phi}{\rho_o} \nabla \rho' \times \nabla \sigma. \quad (6)$$

Here π is the Bernoulli function

$$\pi = \frac{|\mathbf{u}|^2}{2} + \frac{p}{\rho_o} + \frac{\rho'}{\rho_o} \Phi, \quad (7)$$

and $\mathbf{F}$ is the (nonconservative) frictional force per unit mass in the Boussinesq momentum equation

$$\frac{\partial \mathbf{u}}{\partial t} = -\omega \times \mathbf{u} - \nabla \pi + \mathbf{F}, \quad (8)$$

where p is the deviation of the pressure from that of a resting, hydrostatically balanced ocean; ρ_o is a reference density; ρ' is the departure of the in situ density from the reference ρ_o; and Φ is the geopotential.

Equation (6) is the form of the generalized PV flux written down in MN92 [see their Eqs. (1b) and (1c)]. Note that in Eq. (6) there is a nonadvective thermobaric term,[4]

$$\frac{\Phi}{\rho_o} \nabla \rho' \times \nabla \sigma.$$

This term is discussed at length in M01, does not make a large contribution, but is diagnosed and retained here for completeness.

The PV flux form written out in Eq. (5) has great utility[5] and will be a primary focus in the present study for the following reasons.

(i) It reveals the impermeability theorem in a transparent and direct way: the first term on the rhs, when projected in the direction normal to the σ surface, is equal to $v_\sigma \rho Q$, where $v_\sigma = -|\nabla \sigma|^{-1} \partial \sigma / \partial t$ is the velocity of the σ surface normal to itself.[6] The remaining terms represent a flux that is always parallel to the σ surface. Thus (see Czaja and Hausmann 2009), the mass-weighted PV content of an isopycnal layer can only be changed by fluxes where the layer intersects a boundary.

(ii) It shows that $\mathbf{J}$ can be evaluated without explicit reference to frictional ($\mathbf{F}$) and buoyancy ($D\sigma/Dt$) sources and thermobaric effects. Knowledge of the circulation and pressure field is all that is required. We will see that this is particularly true in the present application, because we have an intense interest in the $\mathbf{J}$ vector near the sea surface, where $\mathbf{F}$ and ($D\sigma/Dt$) are large but difficult to evaluate.

(iii) It shows that in the steady state the Bernoulli function π is the streamfunction for the $\mathbf{J}$ vector on σ surfaces, even in the presence of friction ($\mathbf{F}$) and buoyancy ($D\sigma/Dt$) sources. This is a very general result, first noted by Schär (1993) and Bretherton and Schär (1993). Thus, where the π contours on σ surfaces are close together (wide apart), $\mathbf{J}$ is large (small).

Finally, using Eq. (5) the vertical component of the PV flux, $J_z = \mathbf{k} \cdot \mathbf{J}$ is given by

$$J_z = \omega_z \frac{\partial \sigma}{\partial t} + \mathbf{k} \cdot \left(\frac{\partial \mathbf{u}}{\partial t} + \nabla \pi \right) \times \nabla \sigma, \quad (9)$$

where $\mathbf{k}$ and ω_z are the unit vector and the component of the absolute vorticity in the vertical direction. As discussed in M01, it can be written succinctly as [see their Eq. (14)]

$$J_z = \omega_z \left(\frac{\partial \sigma}{\partial t} + \mathbf{u}_A \cdot \nabla \sigma \right) \quad (10)$$

In which

$$\mathbf{u}_A = \frac{1}{\omega_z} \mathbf{k} \times \left(\frac{\partial \mathbf{u}}{\partial t} + \nabla \pi \right) \quad (11)$$

is a generalized geostrophic velocity $\mathbf{u}_A$.

Having briefly reviewed the theoretical background, we now use it to map the circulation of PV around the gyre, by drawing π contours on σ surfaces. We use the near-surface vertical flux of PV to diagnose the processes that extract PV from the ocean circulation, generating mode waters.

4. Diagnosing interior and mixed layer PV flux vectors

a. Interior circulation of PV

Figure 5 shows the potential vorticity and Bernoulli contours plotted on the EDW/STMW core isopycnal ($\sigma = 26.4$ kg m^{-3}) at depths below 100 m. In December (Fig. 5a) the STMW low PV core is clearly visible in the northwestern part of the subtropical gyre, just south of

---

[4] The term is identically zero if $\sigma = \sigma(\rho')$: for example, if we ignore the pressure dependence of ρ' on p, this is a very good approximation in the present application, where we consider processes at or near the sea surface.

[5] We note in passing that, on equating Eqs. (5) and (6), we obtain the component of the momentum equation in the σ surface, written out as Eq. (7) in M01.

[6] Explicitly, $(\omega \partial_t \sigma) \cdot \nabla \sigma |\nabla \sigma|^{-1} = (\omega \cdot \nabla \sigma) \partial_t \sigma |\nabla \sigma|^{-1} = \rho Q v_\sigma$.

the Gulf Stream. Bernoulli contours indicate a closed anticyclonic circulation of PV around the gyre. At this time, the EDW layer outcrops in the mideastern part of the basin and is migrating southward. In March (Fig. 5b) the mixed layer reaches down into the EDW layer (potential density contours at the surface and at a depth of 100 m are coincident with one another, indicating the presence of a mixed layer). Strong upward vertical PV fluxes indicate that PV is being drawn out of the layer (see next section). Previously closed horizontal Bernoulli contours are now open and thread into the mixed layer. In June (Fig. 5c) the surface EDW outcrop has migrated northward to 45°/50°N, but at 100 m the EDW layer remains centered on its winter position. We note that the PV flux is stronger than in prewinter conditions because the Bernoulli contours are closer together than in December. In September (Fig. 5d), Bernoulli contours have almost returned to their prewinter positions with closed π contours encircling the EDW core. Note how the entire EDW PV signature has been enhanced (has lower PV) relative to December of the previous year. This is also true of Madeira Mode Water in the eastern part of the basin.

b. Vertical flux of PV in the mixed layer and its seasonal cycle

We are interested in evaluating the vertical PV flux at or near the sea surface and establishing which processes set its magnitude and pattern. Previous studies (see, e.g., MN92) have employed an approximate form of Eq. (6) evaluated at the sea surface using air–sea buoyancy fluxes and surface wind stresses. However, progress is only possible if rather strong assumptions are made about the mixed layer properties to enable one to infer body momentum and buoyancy forcing from surface fluxes alone. Although very useful, permitting global scale maps to be made using satellite data as in Czaja and Hausmann (2009), here we prefer to proceed from Eq. (10) because fewer assumptions need to be made in its application.

In the following plots, the first term on the rhs of Eq. (10) is computed using the equation of state and OCCA estimates of temperature and salinity tendencies; the second term on the rhs uses in situ pressure anomaly and geopotential. We neglect the velocity tendency term because at this coarse resolution the Rossby number is always very small. This explicit method, employing full knowledge of the three-dimensional flow fields, allows one to map out the vertical component of the **J** vector.

Figure 6 shows the 2004–06 time series of J_z averaged over the box shown in Fig. 1. The vertical PV flux is almost entirely confined to the mixed layer, whose depth is shown by the thick green line. That J_z is confined to the mixed layer is a common feature and occurs at all

locations. A supporting scaling argument is given in MN92. A positive flux at the sea surface induces a vertical PV flux divergence over the depth of the mixed layer, thus decreasing the PV [see Eq. (2)] and deepening the mixed layer. A positive J_z (negative) coincides with the time when the mixed layer deepens (shoals). Note that the mixed layer depth shown in Fig. 6 does not exactly match the depth of the vertical PV flux layer. This is due to both the box averaging employed and to the sensitivity of the MLD calculation, which can lead to uncertainties in MLD by several meters.

An interesting observation from Fig. 6 is that, over the first hundred meters or so of the ocean, winter and summertime vertical PV fluxes are almost in balance. This is because wintertime negative fluxes are balanced by summertime fluxes associated with the buildup of the seasonal thermocline. Below this compensation depth the net annual PV flux is clearly positive (i.e., out of the ocean). Below, we will make use of this observation to map PV fluxes over the EDW/STMW outcrop.

From Eq. (10) it is possible to decompose the vertical PV flux into a potential density tendency term and an advective term. The potential density tendency component is found to dominate over advection (not shown). Under the assumption that the mixed layer density tendency is in turn dominated by air–sea buoyancy fluxes, the vertical PV flux reaching the bottom of the mixed layer—and thus influencing the ocean interior—is primarily driven by air–sea buoyancy fluxes.

To relate the vertical PV flux to the EDW and STMW seasonal cycle, in Fig. 6 we also plot time series of (i) the local EDW/STMW isopycnal layer depth {low, intermediate, and high values of $\sigma = [26.2, 26.4, 26.6]$ kg m^{-3}}, (ii) the local EDW formation rate due to air–sea buoyancy fluxes, and (iii) the mixed layer vertical PV flux divergence. Note that the formation rate time series is zero (not zero) on days when the density of the sea surface (or equivalently the mixed layer) is outside (inside) the range of the EDW layer while the time integral yields the rate averaged over the box shown in Fig. 1.

The box-average quantities shown in Fig. 6 are located in the EDW/STMW core (see Figs. 3, 4) and coincide with a region of net positive EDW formation rate (see Fig. 1). The positive phase of EDW formation corresponds to a time when, under air–sea buoyancy loss conditions, the southern edge of the EDW outcrop migrates southward faster than the cold northern edge, which is pinned along the path of the Gulf Stream [see a more detailed discussion in Maze et al. (2009)]. In contrast, the negative phase of EDW formation (destruction) corresponds to a time when, under buoyancy gain conditions, the warm southern edge of the EDW outcrop returns northward faster than the cold northern
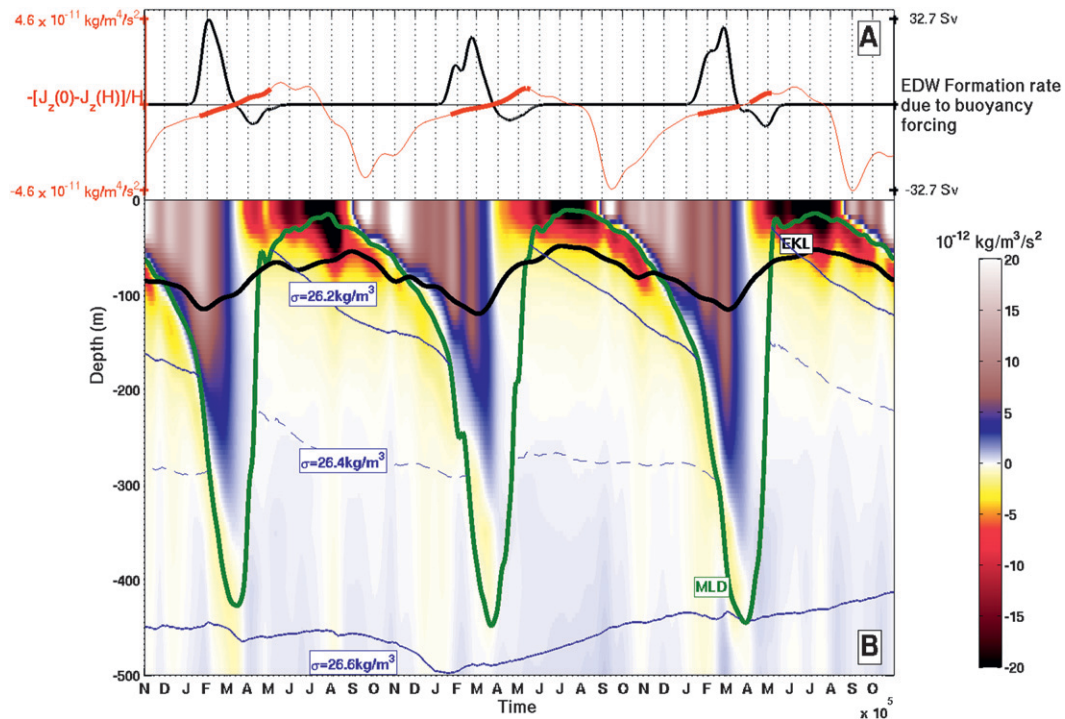
FIG. 6. (a) The thick black line is the 2004–06 daily EDW formation rate due to surface buoyancy forcing for which the maximum amplitude is indicated in Sv on the black scale on the right. The red line is the 2004–06 daily vertical PV flux divergence over the mixed layer, $-(J_z^{z=0} - J_z^{z=H})H^{-1}$, where H is the MLD and for which the maximum amplitude is indicated in kg m^{-4} s^{-2} on the left. The thick red portion of the curve highlights days when the ML density is in the range of EDW. (b) The 2004–06 daily time series of the vertical PV flux, $J_z = f\partial_t\sigma + \mathbf{k} \cdot \mathbf{V}\pi \times \mathbf{V}\sigma$, between -500 m and the sea surface, averaged over the region indicated by a black box in Fig. 1. The units are 10^{-12} kg m^{-3} s^{-2}, with a color scale located on the right. The thick green (black) line is the box-averaged mixed (Ekman) layer depth. Blue lines give the isopycnal depth averaged over the box: thick lines are $\sigma = [26.2, 26.6]$ kg m^{-3} and thin dashed lines are $\sigma = 26.4$ kg m^{-3}.

edge of the outcrop. Beginning from its position co-incident with the path of the Gulf Stream west of 50°W, it takes about two months for the warm outcrop to reach its southernmost position, whereas in a matter of only two weeks or so it returns to its initial position to the north. This is why there is a net annual formation (a volume increase) of EDW over this region.

The central role played by the migration velocity of outcropping isopycnals in setting the formation rate is reminiscent of the mixed layer depth cycle: the ML deepens more slowly than it shoals and is the key to understanding the origin of the low PV of STMW. Indeed, one observes that, during the mixed layer deepening phase, the vertical PV flux acts to reduce the PV in the mode water layer because the mixed layer penetrates the layer without reaching its deepest isopycnal. On the other hand, when the seasonal thermocline shoals, the restratification process injects high PV into the STMW layer (see the mixed layer PV tendency in Fig. 6). Because the former phase persists for a longer time than the latter, the EDW layer experiences a wintertime net

PV reduction forming STMW. There is thus a clear connection between, from one perspective, air–sea buoyancy flux and EDW formation rates and, from another, the vertical PV flux and STMW formation.

c. Accumulated effects of vertical PV fluxes on EDW

It is highly instructive to make use of a Lagrangian perspective to investigate the seasonal cycle of PV fluxes experienced by EDW/STMW. This can be done by, as in the Walin formalism, following the outcrops around as they migrate meridionally and focusing on the integrated flux through the outcrop window. Following the approach explored for the buoyancy flux over the EDW outcropping region in Maze et al. (2009), one can map the vertical PV flux given by Eq. (10). We define

$$\mathcal{J}_z(X_i, h) = \int_{X_j} J_z(t, x, y, z = h)\mathcal{H}_{mld}^h(t, x, y)\, dX_j, \qquad (12)$$

where (t, x, y, z) are the time, zonal, meridional, and vertical axes. A spatial average is obtained by setting

$X_i = t$ and $X_j = (x, y)$; a temporal average by setting $X_i = (x, y)$ and $X_j = t$. The outcrop mapping function $\mathcal{H}^h_{\mathrm{mld}}$ is given by

$$\mathcal{H}^h_{\mathrm{mld}}(t, x, y) = \begin{cases} 1, & \text{if} \begin{bmatrix} \sigma_{\mathrm{EDW}} - \dfrac{\delta\sigma}{2} < \sigma(z = h) \\ \sigma(z = h) \leq \sigma_{\mathrm{EDW}} + \dfrac{\delta\sigma}{2} \\ \mathrm{mld} \leq h \end{bmatrix} \\ 0, & \text{otherwise,} \end{cases} \quad (13)$$

where mld stands for mixed layer depth. This is a binary function that has a value of unity when the potential density at depth h is in the EDW outcrop range $\sigma_{\mathrm{EDW}} \pm \delta\sigma$ (and has thus been penetrated by the mixed layer) and zero otherwise. The mixed layer depth criterion ensures that the mapping is restricted to times when the outcrop at depth h is in direct contact with the atmosphere and thus remains a surface outcropping region. At the surface ($h = 0$), the function $\mathcal{H}^0_{\mathrm{mld}}$ reduces to the EDW surface outcrop region.

Figure 7 shows $\mathcal{J}_z(x, y, h = 100\,\mathrm{m})$ and its potential density tendency and advective components for 2004–06. Here $h = 100$ m was chosen because this is the shallowest depth that the wintertime PV flux cannot be compensated by the summertime PV flux building the seasonal thermocline (see discussion in the previous section). It should also be noted that it corresponds to the depth at which STMW is capped in summer (see Fig. 3). Mapping the vertical PV flux in this way thus focuses on those fluxes that influence the STMW core—our primary interest.

The potential density tendency component of the vertical PV flux (Fig. 7a) is directed upward (positive) almost everywhere in the outcropping area. This term is driven by air–sea buoyancy flux, that is, primarily by surface cooling. It is very large along the path of the Gulf Stream to the north of the STMW core. However, we observe a southward extension of large positive PV flux from the Gulf Stream to a latitude of about 33°N (the latitude of the zonal section shown in Fig. 4) between 60° and 45°W. This southward extension is located over the STMW core and is in direct contact with the low PV bowl of mode water in winter. This is not the case for the high PV fluxes along the Gulf Stream. We note that this component of the PV flux is also slightly negative on the northern edge of the outcropping area and along the Gulf Stream from the U. S. East Coast to 70°W. The advective component of the vertical PV flux (Fig. 7b) shows a different pattern. It is positive along the Gulf Stream path and negative elsewhere over the EDW outcrop. The total vertical PV flux (Fig. 7c) is therefore dominated by the potential density tendency. The region
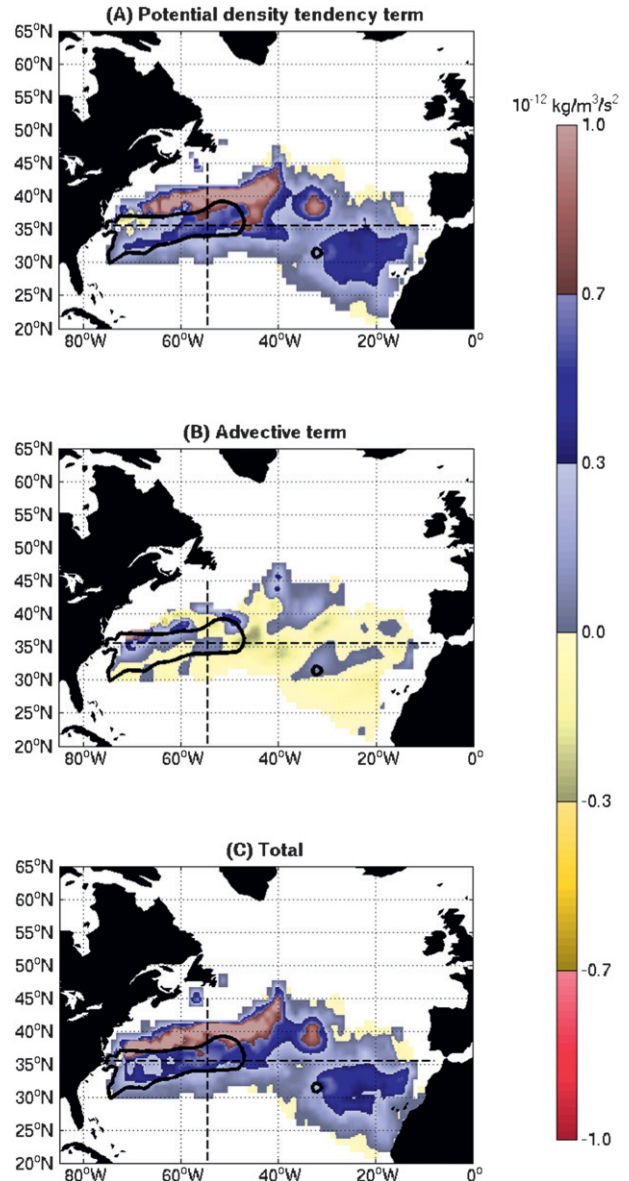
FIG. 7. The 2004–06 time mean of contributions to the vertical PV flux: (a) potential density tendency $f\partial_t\sigma$, (b) advective $\mathbf{k} \cdot \mathbf{V}\pi \times \mathbf{V}\sigma$, and (c) their sum mapped according to Eq. (12) using $h = 100$ m. All PV fluxes have thus been restricted to the $\sigma_{\mathrm{EDW}} = 26.4 \pm 0.2$ kg m^{-3} isopycnal layer at a depth of 100 m when penetrated by the ML. Black contours indicate the region of maximum net formation rate of EDW.

of maximum EDW volume change rate (a southwest–northeast band south of the Gulf Stream indicated by the black contours in Fig. 7) occurs where the STMW core is directly sustained by wintertime loss of PV.

The region of largest vertical PV flux along the Gulf Stream path is localized somewhat to the north of the STMW core. Referring to the Bernoulli contours, shown

in Fig. 5, mapping the circulation of PV in the ocean interior, we observe the following.

- Bernoulli contours parallel to the Gulf Stream core advect a fraction of the low PV water being formed there away from the core of STMW.
- The low PV water being formed south of the Gulf Stream and north of 33°N between 60° and 45°W intersects Bernoulli contours on the southern flank of the Gulf Stream. These are closed and circulate around the gyre through the STMW core and can readily sustain it.
- The low PV water being formed along the Gulf Stream from the U. S. East Coast up to 60°W by advective fluxes is advected east and southeast toward the STMW core.

d. Role of the mechanical forcing

We now consider the relative importance of mechanical and diabatic forcing in sustaining the STMW bowl of low PV. The Walin formalism focuses entirely on buoyancy and so cannot directly address this issue. Instead, the PV framework applied here admits the possibility that mechanical forcing can also create low PV. For example, downstream winds blowing over the Gulf Stream (Thomas 2005; Joyce et al. 2009) could drive heavy fluid over light, triggering convection and thus acting as a source of low PV [see the $\mathbf{F} \times \nabla \sigma$ term in Eq. (6)]. So, is STMW low PV primarily sustained by a quasi-vertical diabatic process due to local air–sea buoyancy fluxes and/or does mechanical forcing also play a significant role?

This question is not immediately addressed by diagnoses of the vertical PV flux based on Eq. (10) because it derives from Eq. (5) where mechanical and diabatic forcing components are not explicit. Instead, note that at the sea surface the vertical velocity vanishes and so the vertical PV flux written in the form Eq. (6) does clearly expose the relative contribution of diabatic and mechanical components. Remember that expressions Eqs. (5) and (6) are exactly equivalent to one another. Thus, we can estimate the vertical mechanical PV flux using Eq. (6) and compare it to the total flux given by Eq. (10) mapped in the previous section.

We write the body force as

$$\mathbf{F} \simeq \frac{1}{\rho_0} \frac{\partial \boldsymbol{\tau_s}}{\partial z}, \qquad (14)$$

where ρ_0 is a reference density and $\boldsymbol{\tau_s}$ is the wind stress vector at the sea surface. If we further assume that the layer experiencing a significant stress is the Ekman layer—with depth $\delta_e = 0.7 f^{-1} \sqrt{|\tau| \rho^{-1}}$ determined

using a formulation of the turbulent friction velocity $u^* = \sqrt{|\tau| \rho^{-1}}$ (see, e.g., Cushman-Roisin and Manga 1994) and the numerical factor 0.7 used in the KPP scheme in OCCA—then the vertical mechanical PV flux at the surface reduces to

$$J_s^{\text{mech}} = \mathbf{k} \cdot \left(\frac{\boldsymbol{\tau_s}}{\rho_0 \delta_e} \times \nabla \sigma \right). \qquad (15)$$

This vertical PV flux is simply linked to the advection of density by the Ekman drift.

We adopt the Lagrangian method used in section 4c to define a mean map and a time series of the mechanical PV flux experienced by the EDW layer at depth h as

$$\mathcal{J}_s^{\text{mech}}(X_i, h) = \int_{X_j} J_s^{\text{mech}}(t, x, y) \mathcal{H}_{\text{ekl}}^h(t, x, y) \, dX_j, \qquad (16)$$

where the outcrop binary mapping function $\mathcal{H}_{\text{ekl}}^h$ is the same as $\mathcal{H}_{\text{mld}}^h$ given by Eq. (13), but using the Ekman layer depth in place of the mixed layer depth.

To focus on the mechanically induced vertical PV flux influencing the STMW layer, we map it at a depth of 100 m, for the reasons discussed in the previous section. In Fig. 8a, we show the 2004–06 mean map of $\mathcal{J}_s^{\text{mech}}(x, y, h = 100 \, \text{m})$. The mechanical PV flux is predominantly positive over the outcrop with a maximum along the Gulf Stream path where the vector product of strong westerlies and meridional density gradient is particularly large. On the southern edge of the pattern, along the southern flank of the subtropical gyre, the PV flux is also positive because the meridional density gradient is again directed northward and winds have not yet reversed sign into easterlies (the zero wind line occurs around 30°N).

In Fig. 8b, the 2004–06 cumulative time series is shown, but plotted as a typical year (averages of all Januaries, Februaries, etc.) of $\mathcal{J}_s^{\text{mech}}(t, h = 100 \, \text{m})$ (red curve) and $\mathcal{J}_z(t, h = 100 \, \text{m})$ (black curve). Both indicate that vertical PV fluxes ventilate the STMW layer from January to the end of March. During the remainder of the year neither the mixed layer nor the Ekman layer penetrates significantly into the STMW layer, and the accumulated PV flux remains flat. The net integrated total PV flux at the end of the year is $4.7 \times 10^7 \, \text{kg m}^{-1} \, \text{s}^{-1}$ of which mechanical forcing contributes $0.6 \times 10^7 \, \text{kg m}^{-1} \, \text{s}^{-1}$, about 13% of the total.

Before going on, a note of caution is in order. The coarseness of the resolution of the analyzed oceanographic (OCCA) fields used here makes it very difficult to directly assess the role of the interaction of winds and fronts because it is not resolved. At this time, similar
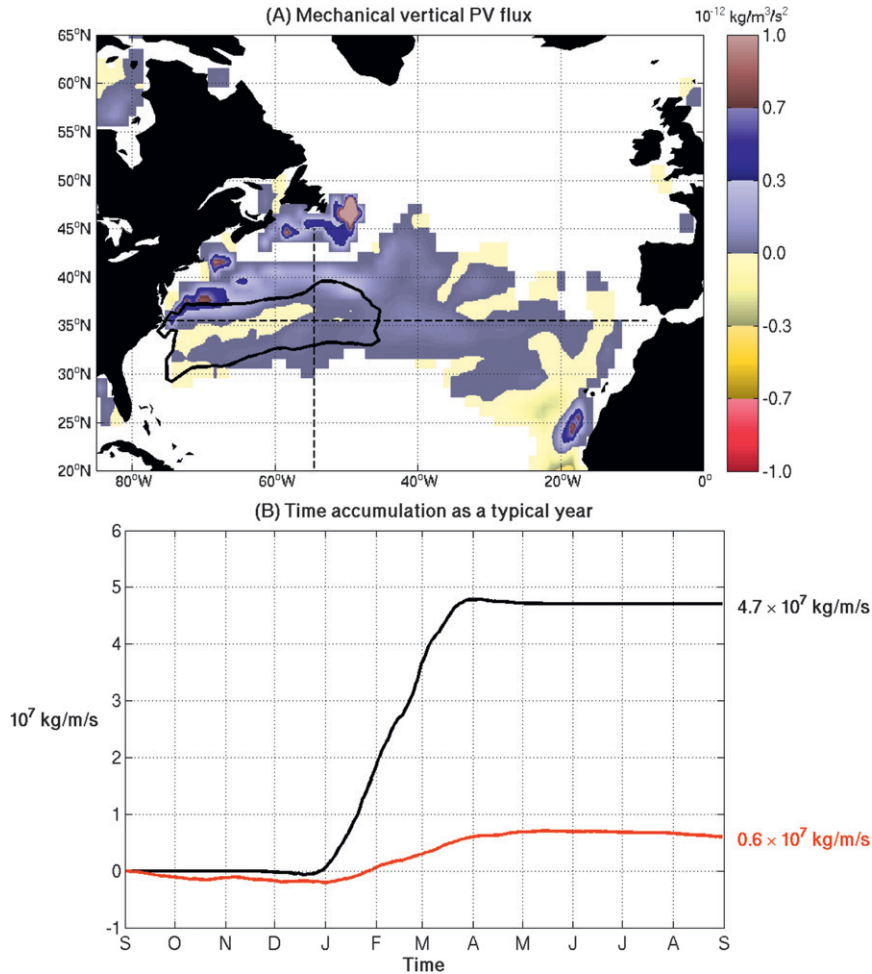
FIG. 8. (a) The 2004–06 mean vertical PV flux due to mechanical forcing over the EDW outcrop computed from Eq. (17) using $\mathcal{H}_{ekl}^{h=100m}$. (b) Time integrals over 2004–06, plotted as typical years, of the total (black) and mechanical (red) vertical PV fluxes in the EDW layer at a depth of 100 m. Net values are also indicated.

diagnostics are not yet available with realistic high-resolution datasets. The estimate presented here should be considered as a first step toward a better quantitative understanding of the wind–front interaction role in STMW dynamic.

e. Residence time

We can compute an implied residence time for STMW by (i) integrating mass-weighted potential vorticity ρQ over the volume of fluid contained within the $Q \leq 1.5 \times 10^{-10}$ m^{-1} s^{-1} surface and finding its maximum annual value and (ii) dividing this quantity by the accumulated total PV flux over the annual cycle. The annual maximum mass-weighted potential vorticity integrated over the STMW layer is 1.67×10^8 kg m^{-1} s^{-1} (a value reached in May). The accumulated total PV flux over an annual cycle (illustrated in Fig. 8b) is 4.71×10^7 kg m^{-1} s^{-1}. We thus

obtain a STMW residence, or turnover, time of 3.54 yr. This value is in very good agreement with the 3.57 ± 0.54 yr observational estimate of Kwon and Riser (2004) and of the same order of magnitude as the oxygen-based estimate of o(3.17 yr) from Jenkins (1982).

5. Discussion: Implication for mode water formation mechanisms

In this paper, we have employed potential vorticity theorems to frame and quantify the process of mode water formation, providing a complementary perspective from that of Walin which places emphasis on buoyancy. Iso-pycnal maps of the distribution and circulation of low potential vorticity tagging STMW were presented and described in relation to the seasonal migration of outcrops and the mixed layer cycle. Furthermore, making use of
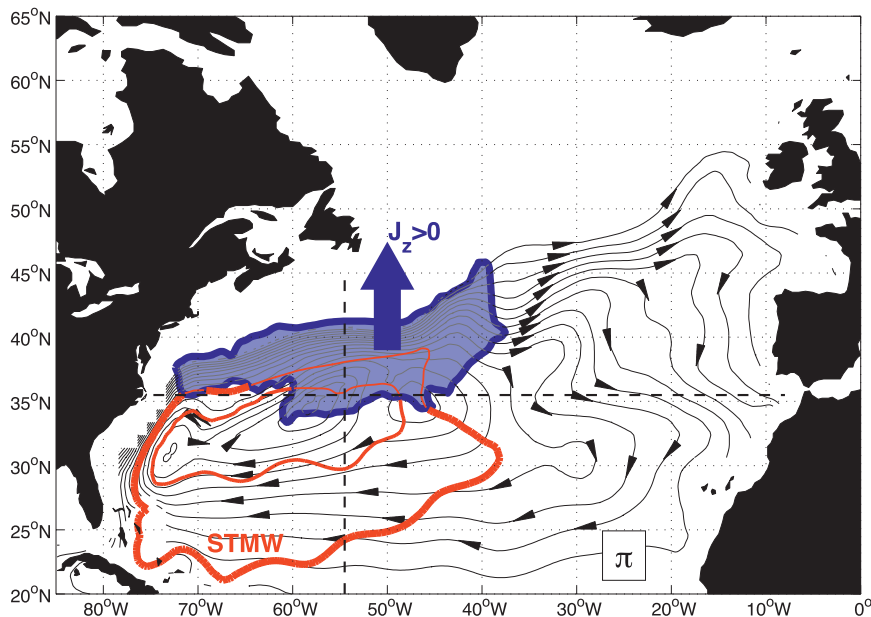
FIG. 9. Simplified view of the main results of this study. The blue area is the dominant positive vertical PV flux area $[\mathcal{J}_z(x, y, h = 100\,\text{m}) = 0.45\,\text{kg}\,\text{m}^{-3}\,\text{s}^{-2}]$ from Fig. 7c. Black contours with arrows indicates mean PV flux streamlines (2004–06 time-mean Bernoulli contours on the $\sigma_{\text{EDW}} = 26.4\,\text{kg}\,\text{m}^{-3}$ isopycnal). Red contours indicate the STMW subset of EDW {two PV contours of $Q = [0.6; 1.5] \times 10^{-10}\,\text{m}^{-1}\,\text{s}^{-1}$ on σ_{EDW}}.

the flux form of the PV conservation equation and the impermeability theorem, we were able to diagnose where and when vertical PV fluxes draw PV out of the EDW layer. We found that STMW low PV waters are primarily sustained by a vertical PV flux in the mixed layer driven by air–sea buoyancy fluxes, with mechanical (wind) forcing playing a secondary role.

Figure 9 summarizes key results of our study. It shows the annual-mean Bernoulli function on the $\sigma = 26.4\,\text{kg}\,\text{m}^{-3}$ surface, threading through the mode water layer, with arrows indicating the sense of circulation around the pool of low PV water within the area marked by the red contour. The area, shaded blue, centered on and to the south of the Gulf Stream indicates where potential vorticity is extracted from the mode water layer. Potential vorticity removal occurs on the northern flank of the low PV pool, just south of the Gulf Stream. In our estimates, buoyancy loss inducing vertical PV fluxes in the mixed layer play the primary role in potential vorticity loss, exceeding the contribution due to mechanical forcing by the wind.

It should be emphasized, however, that the annual-mean picture shown in Fig. 9 masks the central importance of the seasonal cycle in the PV extraction process. PV loss occurs primarily in wintertime when the mixed layer deepens sufficiently to access the mode water pool, allowing PV to be fluxed out through the sea surface,

parallel to the almost vertical isopycnal surfaces. Once restratification occurs and the isopycnal surfaces again bury the low PV water, flux out of the ocean is prohibited by the impermeability theorem. We estimate a residence time for STMW of 3.54 yr based on the ''head'' of STMW and the magnitude of the PV loss integrated over the outcrop.

Before finishing, we should mention key aspects of the mode water formation process that are not addressed in our study. Key among them is the role of eddy and frontal processes in STMW formation. The ocean state estimates employed here do not resolve the eddy field and, instead, smooth out small scales. It seems likely that processes on the scale of the oceans mesoscale play a role modulating air–sea interaction, promoting convection and hence creation of low PV (see Cerovecki and Marshall 2008). Moreover, winds directed in the downstream direction of intense surface fronts may, for short periods when all is aligned, extract very large amounts of PV (Thomas 2005; Joyce et al. 2009). But, their integrated effect as yet remains unclear and our calculations here are likely to underestimate their role. Further analysis using realistic eddy resolving datasets is thus required to achieve a quantitative comparison between mechanical and buoyancy forcing of low PV mode waters in the presence of eddies.

Finally, the study of Czaja and Hausmann (2009) found different roles of mechanical and diabatic fluxes in PV entry/exit in the subpolar gyre between the North Pacific and North Atlantic, whereas in the subtropical gyre their respective roles were similar. The methods employed here, which focused on EDW and STMW, could be used to view the global input and output of potential vorticity in many other density layers and could help investigate differences found by Czaja and Hausmann.

REFERENCES

Brambilla, E., L. D. Talley, and P. E. Robbins, 2008: Subpolar Mode Water in the northeastern Atlantic. Part II: Origin and transformation. *J. Geophys. Res.,* **113,** C04026, doi:10.1029/2006JC004063.

Bretherton, C. S., and C. Schär, 1993: Flux of potential vorticity substance: A simple derivation and a uniqueness property. *J. Atmos. Sci.,* **50,** 1834–1836.

Cerovecki, I., and J. Marshall, 2008: Eddy modulation of air–sea interaction and convection. *J. Phys. Oceanogr.,* **38,** 65–83.

Cushman-Roisin, B., and M. Manga, 1994: *Introduction to Geophysical Fluid Dynamics.* Prentice Hall, 320 pp.

Czaja, A., and U. Hausmann, 2009: Observations of entry and exit of potential vorticity at the sea surface. *J. Phys. Oceanogr.,* **39,** 2280–2294.

Forget, G., 2010: Mapping ocean observations in a dynamical framework: A 2004–06 ocean atlas. *J. Phys. Oceanogr.,* **40,** 1201–1221.

——, G. Maze, M. Buckley, and J. Marshall, 2011: Estimated seasonal cycle of North Atlantic Eighteen Degree Water volume. *J. Phys. Oceanogr.,* **41,** 269–286.

Hanawa, K., and L. Talley, 2001: Mode waters. *Ocean Circulation and Climate: Observing and Modelling the Global Ocean,* G. Siedler, J. Church, and J. Gould, Eds., Academic Press, 373–386.

Haynes, P., and M. McIntyre, 1987: On the evolution of vorticity and potential vorticity in the presence of diabatic heating and frictional or other forces. *J. Atmos. Sci.,* **44,** 828–841.

Jenkins, W. J., 1982: Oxygen utilization rates in North Atlantic subtropical gyre and primary production in oligotrophic systems. *Nature,* **300,** 246–248, doi:10.1038/300246a0.

Joyce, T. M., L. N. Thomas, and F. Bahr, 2009: Wintertime observations of Subtropical Mode Water formation within the Gulf Stream. *Geophys. Res. Lett.,* **36,** L02607, doi:10.1029/2008GL035918.

Keffer, T., 1985: The ventilation of the world's oceans: Maps of the potential vorticity field. *J. Phys. Oceanogr.,* **15,** 509–523.

Kwon, Y., and S. Riser, 2004: North Atlantic subtropical mode water: A history of ocean-atmosphere interaction 1961–2000. *Geophys. Res. Lett.,* **31,** L19307, doi:10.1029/2004GL021116.

Marshall, J., and J. G. Nurser, 1992: Fluid dynamics of oceanic thermocline ventilation. *J. Phys. Oceanogr.,* **22,** 583–595.

——, A. Adcroft, C. Hill, L. Perelman, and C. Heisey, 1997a: A finite-volume, incompressible Navier Stokes model for studies of the ocean on parallel computers. *J. Geophys. Res.,* **102** (C3), 5753–5766.

——, C. Hill, L. Perelman, and A. Adcroft, 1997b: Hydrostatic, quasi-hydrostatic, and nonhydrostatic ocean modeling. *J. Geophys. Res.,* **102** (C3), 5733–5752.

——, D. Jamous, and J. Nilsson, 1999: Reconciling thermodynamic and dynamic methods of computation of water-mass transformation rates. *Deep-Sea Res.,* **46,** 545–572.

——, ——, and ——, 2001: Entry, flux and exit of potential vorticity in ocean circulation. *J. Phys. Oceanogr.,* **31,** 777–789.

——, and Coauthors, 2009: The CLIMODE field campaign: Observing the cycle of convection and restratification over the Gulf Stream. *Bull. Amer. Meteor. Soc.,* **90,** 1337–1350.

Maze, G., G. Forget, M. Buckley, J. Marshall, and I. Cerovecki, 2009: Using transformation and formation maps to study the role of air–sea heat fluxes in North Atlantic Eighteen Degree Water formation. *J. Phys. Oceanogr.,* **39,** 1818–1835.

McDowell, S., P. Rhines, and T. Keffer, 1982: North Atlantic potential vorticity and its relation to the general circulation. *J. Phys. Oceanogr.,* **12,** 1417–1436.

Schär, C., 1993: A generalization of Bernoulli's theorem. *J. Atmos. Sci.,* **50,** 1437–1443.

Speer, K. G., and E. Tziperman, 1992: Rates of water mass formation in the North Atlantic Ocean. *J. Phys. Oceanogr.,* **22,** 93–104.

Thomas, L., 2005: Destruction of potential vorticity by winds. *J. Phys. Oceanogr.,* **35,** 2457–2466.

Walin, G., 1982: On the relation between sea-surface heat flow and thermal circulation in the ocean. *Tellus,* **34,** 187–195.

Worthington, L. V., 1959: The 18° Water in the Sargasso Sea. *Deep-Sea Res.,* **5,** 297–305.

——, 1972: Negative oceanic heat flux as a cause of water-mass formation. *J. Phys. Oceanogr.,* **2,** 205–211.

——, 1976: *On the North Atlantic Circulation.* The Johns Hopkins University Press, 110 pp.

Wunsch, C., and P. Heimbach, 2007: Practical global oceanic state estimation. *Physica D,* **230** (1–2), 197–208.